SCIENCE CHINA
Physics, Mechanics & Astronomy

Piezo-/ferroelectric phenomena in biomaterials: A brief review of recent progresses and perspectives

Sun Yao, Zeng Kaiyang and Li Tao

Citation: SCIENCE CHINA Physics, Mechanics & Astronomy; doi: 10.1007/s11433-019-1500-y

View online: http://engine.scichina.com/doi/10.1007/s11433-019-1500-y

Published by the Science China Press

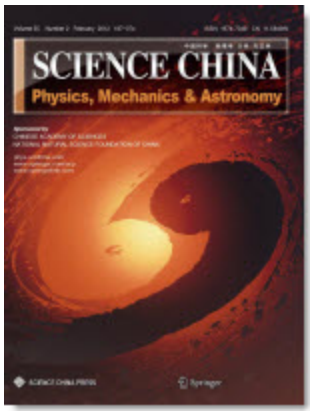

Piezo-/ferroelectric phenomena in biomaterials: A brief review of recent progresses and perspectives

Journal:	*SCIENCE CHINA Physics, Mechanics & Astronomy*
Manuscript ID	SCPMA-2019-0511.R1
Manuscript Type:	Invited Review
Date Submitted by the Author:	12-Dec-2019
Complete List of Authors:	Sun, Yao; Department of Mechanical Engineering Zeng, Kaiyang; Department of Mechanical Engineering Li, Tao; Department of Materials Science and Engineering
Keywords:	Biomaterial, Electromechanical Coupling, piezoresponse force microscopy, ferroelectric, piezoelectric
Speciality:	Biophysics

SCIENCE CHINA
Physics, Mechanics & Astronomy

• Review •

January 2020 Vol. No. : 000000
doi: 10.1007/s11433-000-0000-0

Piezo-/ferroelectric phenomena in biomaterials: A brief review of recent progress and perspectives

Yao Sun,[1] Kaiyang Zeng,[1] and Tao Li[2,*]

[1] *Department of Mechanical Engineering, National University of Singapore, Singapore;*
[2] *Center for Spintronics and Quantum Systems, State Key Laboratory for Mechanical Behavior of Materials, School of Materials Science and Engineering, Xi'an Jiaotong University, Xi'an, Shaanxi, 710049, P.R.China.*

Received January 1, 2020; accepted January 1, 2020; published online January 1, 2020

There have been overwhelming observations of piezo-/ferroelectric phenomena in many biological tissues and macromolecules, boosting the development of bio-based smart devices and the applications using electromechanical coupling phenomena in biological systems. The electromechanical coupling is believed to be responsible for various biophysical behaviors and remarkable biomaterial properties. Despite the abundant phenomenal observations, the fundamental understanding of the piezo-/ferroelectric effect in biomaterials/systems and the rational design of biobased macroscopic materials with desired piezoelectric responses are still scarce. In this review, we firstly present remarkable historical events on the development of piezo-/ferroelectricity in biomaterials, followed by a brief overview of the fundamental physics of piezo-/ferroelectricity. The developments of biopiezo-/bioferroelectricity in protein-based biomaterials and their implications are highlighted subsequently. In experimental studies, to identify the intrinsic piezoelectric/ferroelectric properties from other effects or artifacts is usually elusive. This issue is also addressed and discussed in detail, especially using Piezoelectric Force Microscopy (PFM) and spectroscopy techniques to investigate the local piezo-/ferroelectric phenomena in nanostructured materials are highlighted emphatically.

biomaterials, electromechanical coupling, piezoelectric, ferroelectric, Piezoresponse Force Microscopy

PACS number(s): 47.55.nb, 47.20.Ky, 47.11.Fg

Citation: A. Author, B. Author, and C. Author, Sample manuscript for SCPMA, Sci. China-Phys. Mech. Astron. 59, 000000 (2016), doi: 10.1007/s11433-000-0000-0

1 Introduction

Many biomimetic materials are potential candidates for energy harvesting and biocompatible sensors in living organisms. The rich natural properties of biomaterials and biomacromolecules have inspired researchers to unravel their structure-property-functionality relationships and to develop rational strategies for designing smart bio-inspired devices [1-4]. For example, the biomimetic self-assembling peptides can produce a variety of structures, which enables the design for novel electronic, photonic, and energy functionalities based on the supramolecular interactions and assembled molecular structures [5]. Compared to the traditional inorganic materials, biomaterials usually exhibit more flexible mechanics, better solution processabilities, and abilities to be integrated into other devices.

Some functional structures of biomaterials, such as amino acid, peptide and protein display unique electromechanical (EM) coupling properties, by which electrical charges can be produced in the presence of mechanical stress or mechanical strain is developed upon the application of an electrical bias. In such a case, the material exhibits mutual conversion between electrical and mechanical energy. Piezoe-

*Corresponding author (email: taoli66@xjtu.edu.cn)

lectricity, electrostriction, and flexoelectricity are three typical forms of EM coupling [6-10]. In terms of biomaterials, the so-called biopiezoelectricity is caused by EM coupling in organic molecular nanostructures [11]. Biopiezoelectricity should be carefully proclaimed after clarifying the intrinsic piezoelectricity from other EM couplings and experimental factors. For example, the electrostatic effect can also contribute to the measured EM signals when the material is characterized by Scanning Probe Microscopy (SPM) based techniques [12-16]. On the other hand, bioferroelectricity is a phenomenon in which the polar molecules can be switched between two polarization states subjected to an external force or electric field [11, 17-22]. The ferroelectric phenomena in biomaterials show great potential applications in biosensing and disease diagnosis [23]. However, the occurrence of bioferroelectricity in biological systems remains controversial due to the lack of experimental validation even though we have witnessed many research works suggesting ferroelectricity for many biomaterials [24-26]. The origins and functions of bioferroelectricity in biophysical systems are not well clarified, which need to be explored further.

This paper mainly gives a review of piezo-/ferroelectric properties of protein-based biomaterials. Firstly, we present the short historical notes on piezo-/ferroelectricity of biomaterials, followed by a brief overview of the fundamentals of piezo-/ferroelectricity. Subsequently, the latest developments of biopiezo-/bioferroelectricity of protein-based biomaterials and their implications are highlighted. In the following, we discuss the differentiation of intrinsic piezoelectricity from other EM couplings and experimental factors. The applications of Piezoelectric Force Microscopy (PFM) and its Spectroscopy (PFS/SSPFM) techniques in investigating the local piezo-/ferroelectric phenomena in nanostructured materials are evaluated in detail. Finally, we close with an outlook and challenges in the field.

2 Historical notes

In 1783, Galvani firstly discovered the connection between electricity and the mechanical response of biological systems [27]. Using a spark from an electrostatic generator, he produced a twitching movement in the muscles of a dead frog. He then claimed that the muscles of the frog retained innate electricity, the fluid within the nerves, which he described as ‘animal electricity’. Piezoelectricity in biological systems was firstly noticed in 1941 by Martin [28]. He found that when wool fibers (or hairs) were rubbed together, the sign of the electric charges produced depended on the direction of the rubbing. This effect owed to the cuticle cells of the fiber, which were piezo- and pyroelectric [28]. Later on, piezoelectricity was found in a wide variety of biological materials, including woods [29, 30, 31], bone tissues [32, 33], tendons [34], the human pineal gland [35], sea shell structures [22], butterfly wings [36] and teeth [37], and many more. Not long after the discovery of biopiezoelectricity, pyroelectricity was also found in phalanges and hoof tendons of a cow by Lang in 1966 [38]. The identification of pyroelectricity in many biological systems leads to the speculation of the existence of ferroelectricity in biomaterials [11, 39, 40]. There is a fascinating theory developed to relate bioferroelectricity to ion channels, hypothesizing that conformation transited in voltage-dependent ion channels from a ferroelectric state to a super-ionically conducting state [24]. Based on this hypothesis, ferroelectricity was predicted in liquid crystals, nerves, and muscular impulses by von Hippel [41]. Up to now, the biopiezo-/bioferroelectricity has been explored in a large number of biomaterials, including proteins, biopolymers, molecular systems, polysaccharides, organelles, glands, and seashells, bone and many more [11, 24, 32, 35, 42-52].

Protein-based material is among the most prevalent biomaterials, which is seeking new applications after millennia of impacting the daily life of human beings [53]. For example, collagen has been the most widely investigated piezoelectric entity. Type-I collagen is the most abundant form of collagen in the human body, especially in bones, tendons, and skins. Fukada and Yasuda proposed in 1957 that the crystalline micelles of collagen molecules in bones and tendons caused the piezoelectricity [32]. Many research works on piezoelectricity in bones [47, 52, 54-57] and fibril-formed collagens [58-62] have been published in the following years. Elastin, another highly explored protein-based macromolecule in organs such as the skin, blood vessel walls, and the lungs of the human body, has also been reported to be piezoelectric and ferroelectric [63, 64]. Liu and colleagues suggested that the polarization of elastin originated from the monomer level, which was analogous to the polarization in the unit cell of the classical perovskite ferroelectrics [64]. There are many other kinds of biomacromolecules reported to be piezoelectric or ferroelectric [65-75].

Later, the research path went from the macroscopic level (tissue level) to the micro-/nanoscale (microconstituents/macromolecules) level, allowing researchers to get closer sight into the self-assembling processes of biosystems. Over the past two decades, Piezoresponse Force Microscopy (PFM) and Spectroscopy have been well developed in realizing the characterization of the nanoscale EM couplings of various materials, such as semiconductors [76, 77], organic polymers [78, 79], and many biological materials [20, 41, 80-94]. For protein-based biomaterials, dozens of papers have been devoted to characterizing the nanoscale piezoelectricity using PFM [64, 95-97]. There is a rapidly growing number of biological systems exhibiting a wide range of the EM coupling phenomena at the nanoscale level. Some of them are associated with the additional contributions other than piezoelectricity or ferroelectricity, such as electrostriction [10, 98], flexoelectricity [8], and electro-

static effects [99, 100]. The large discrepancies in the reported piezoelectricity and ferroelectricity of biomaterials need to be clarified and investigated thoroughly to synthesize this type of biomimetic material and design novel medical devices with controlled EM coupling.

3 Piezoelectric and ferroelectric effects

3.1 Definition

The direct piezoelectric effect is defined as that electric charges can be generated as a result of a force exerted on the dielectric materials. The centers of the positive and negative charges coincide before the exertion of stress (Fig. 1a). Under the external mechanical stress, the unit cell is deformed, leading to the separation of the centers of the positive and negative charges and formation of electric dipoles (Fig. 1b). The opposite dipoles inside the material cancel each other and fixed charges remain on the surface of the material, as illustrated in Fig. 1c [101]. On the other hand, the converse piezoelectric effect is that the electric field can induce deformation of the dielectric materials.

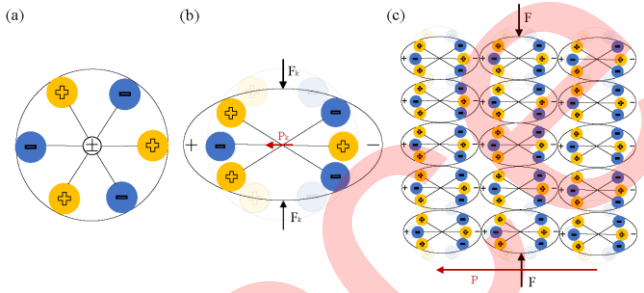

Fig. 1 The direct piezoelectric effect illustrated with a molecular model: (a) The neutralized molecule with no piezoelectric polarization; (b) A mechanical force (F_k) is exerted on the molecule model, resulting in a net polarization (P_k); (c) The polarization on the surface of the material when a force is applied on it [101].

According to the linear theory of piezoelectricity, the generated charge density in a piezoelectric material is proportional to the external stress:

$$P_{pe} = d \times T \quad (1)$$

where P_{pe}, d , T are the polarization vector, piezoelectric strain coefficient, and the stress, respectively. The converse piezoelectric effect can be written as:

$$S_{pe} = d \times E \quad (2)$$

where S_{pe}, and E are the mechanical strain produced by the converse piezoelectric effect and the magnitude of the external electric field.

Biomaterials usually have low-symmetry, highly ordered structures that lack an inversion center. Therefore, piezoelectricity is an intrinsic property of the majority of them [102]. For the protein-based materials, the piezoelectricity usually comes from their basic building blocks or units, i.e., amino acids and peptides, which have been reported to be crystallized since the advent of X-ray diffraction [103]. For instance, lysozyme (widely in tears and saliva) has been reported piezoelectric in its crystalline form [104]. Amino acids crystallize primarily in low symmetric orthorhombic and monoclinic space groups (Fig. 2), except for the large amino acids, L-tryptophan and glycine. Glycine is the non-chiral molecule that does not have an enantiomorphic mirror image. It has three crystalline symmetries, i.e., α, β, and γ forms. The α form is piezoelectrically inactive. So far, the highest piezoelectric responses of amino acid single crystals have been reported to be 178 pC/N in β-glycine and 25 pC/N in hydroxy-L-proline [105, 106]. Except for the intrinsic piezoelectric properties, biomaterials might also exhibit piezoelectric behaviors due to the extrinsic supramolecular interactions. Water molecules may form polarized hydration shells around proteins, leading to a temporary memory effect that accompanies the evolution of polarization in the biomolecule-water systems [107].

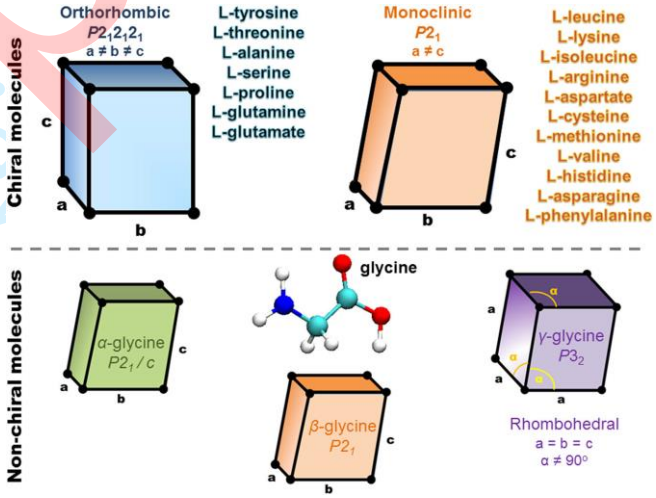

Fig. 2 The crystal symmetries of amino acid crystals [102]. Reproduced with permission. Copyright 2019, Nature Publishing Group.

The ferroelectric effect is defined as the spontaneous electric polarization that can be reversed between at least two stable states by the application of an external electric field [108, 109]. Experimentally, this phenomenon is featured by a typical ferroelectric hysteresis (P-E) loop measured by a Sawyer-Tower circuit, as shown in Fig. 3a. The electric dipoles are usually randomly oriented in the beginning to maintain a minimum energy state. When a positive bias is applied, the net polarization gradually increases and reaches a macroscopic saturated state (P_s) in the direction the same as the positive electric field. The net polarization decreases with reduced positive bias. When the bias is reduced to zero, the ferroelectric material can retain a remnant

polarization P_r. Upon the reversal of electric bias to the negative value, the net polarization gradually decreases to zero, the critical negative electric field is known as the coercive field (E_c). The increase of the negative bias changes the net polarization to the opposite orientation until saturation. The lower half of the ferroelectric hysteresis loop forms as the bias sweeps towards the positive side [110]. Parameters such as saturated polarization (P_s), remnant polarization (P_r), and coercive field (E_c) can be determined from the loop. The material defects may result in an internal field inside the material, resulting in a shift of the ferroelectric hysteresis loop along the axis of the electric field (E), and a large piezoelectric strain ε [111]:

$$\varepsilon = Q(P + \chi E)^2 \approx QP^2 + 2Q\chi PE \quad (3)$$

In this equation, the first term denotes the quadratic electrostrictive strain, and the second term is the linear piezoelectric strain. Q and χ are electrostrictive coefficient and dielectric susceptibility, respectively. Q does not vary much for different materials [109, 111]. The large piezoelectric effect can be aroused by an increase in the large spontaneous polarization (P) and dielectric susceptibility. Therefore, good ferroelectric material is usually a good piezoelectric material as well. The equation can be plotted as a characteristic butterfly loop (Fig. 3b).

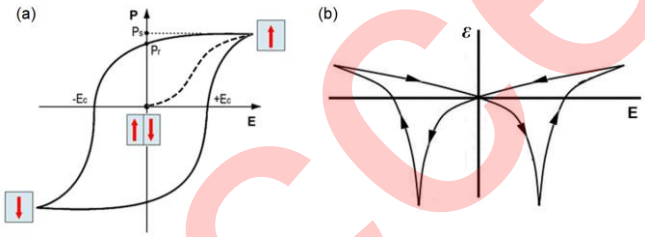

Fig. 3 (a) P-E loop and (b) the butterfly loop that is ideally symmetrical along the bias axis [110]. Reproduced with permission. Copyright 2013, RSC Publishing.

The functional role of ferroelectricity in biology has remained an appealing topic to be explored for a long period. It is suggested that ferroelectricity is of significance in cellular processes [112]. It is also believed that many biological systems have the polarized states and coercive fields to reorient dipoles in them [110]. The ferroelectricity and its functional role in protein-based materials and systems remain poorly explored, despite that we have obtained switchable oriented polar domains in protein structures by applying an external electric field.

3.2 Characterization methods of piezoelectric and ferroelectric properties

Macroscopically, many techniques can be used to identify ferroelectricity, such as measuring phase transition and anomaly in dielectric constant, second harmonic generation (SHG) microscopy, Sawyer-Tower (S-T) circuit, and structural analysis by X-ray diffraction (XRD). In practice, the combinations of various techniques are recommended to study ferroelectricity [113]. The ferroelectric material exhibits phase transition at a signature temperature T_c (the Curie temperature) at which the paraelectric-to-ferroelectric phase transition occurs. It can be characterized by using XRD, differential scanning calorimetry (DSC), and SHG measurements. Sawyer-Tower (S-T) circuit is the typical method to plot the ferroelectric hysteresis (P-E) loop on the macroscopic scale [22, 110, 114]. On the nanoscale, PFM is widely used to characterize the piezoresponse of biomaterials. Its Spectroscopy modes, i.e., Piezoresponse Force Spectroscopy (PFS) and Switching Spectroscopy Piezoresponse Force Microscopy (SSPFM) record the polarization switching dynamics based on phase and amplitude hysteresis loops/maps, which reveal the information of polarization direction reversal and strain variation, respectively [92, 115].

PFM is based on the detection of the EM response induced by the converse piezoelectric effect, ionic movement, or any mechanisms that cause mechanical deformation by applying an electric field. The standard experimental setup is on the base of a commercial SPM equipment with a four-quadrant photodetector, a conductive probe, a function generator and lock-in amplifiers (Fig. 4). The function generator is used to apply an AC voltage to the conductive tip that is in contact with the sample surface. The voltage induced deformation is detected by a laser beam shined at the end of the cantilever and reflected towards a four-quadrant photodiode. The force on the cantilever is kept constant by a feedback loop during the scanning process. By tracking the twisting and deflection of the cantilever motion, the in-plane and out-of-plane signals can be extracted from the lock-in amplifiers. In the vertical PFM (VPFM) mode, the out-of-plane polarization is measured by detecting the deflection of the probe at the selected frequencies. In the lateral PFM (LPFM) mode, the in-plane polarization is detected as the lateral motion of the cantilever due to the bias induced surface shearing [116].

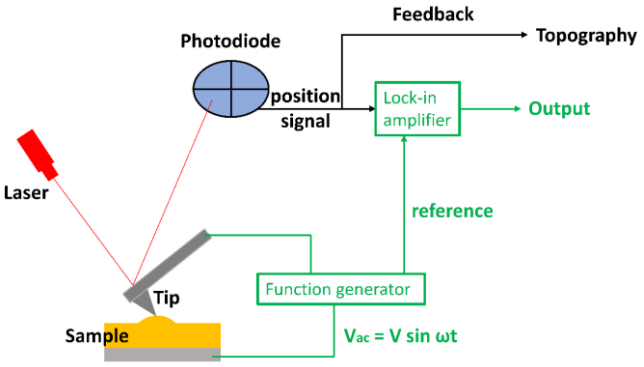

Fig. 4 Schematic diagram of the PFM experimental setup.

PFS is the technique to acquire the local ferroelectric hysteresis loops to study polarization switching dynamics. In this technique, the optimal signal-to-noise ratio is achieved at the frequencies near the contact resonances of the cantilever-sample system. The tip approaches the sample surface in the vertical direction with the deflection setpoint as feedback. When the setpoint is reached, a hysteresis loop starts to be acquired by sweeping the bias. Parameters such as forward and reverse coercive biases, imprint voltage, and saturation response can be extracted from the dataset. During the PFS experiment, the tip is fixed at a given location on the sample surface and an electric wave $V_{tip} = V_{probe}(t) + V_{ac}\cos\omega t$ is applied to the tip (Fig. 5a), where the AC voltage V_{ac} is the PFM driving amplitude. The $V_{probe}(t)$ is comprised of a sequence of DC pulse voltages with the amplitude V_i and duration τ_1 (high state) separated by intervals of zero bias with the duration of τ_2 (low state). The envelope of the voltage pulses is specified by a triangular wave having amplitude V_{max} and period T. The wave repeats N times at a single location. After time $\delta\tau$, the piezoresponse is collected for time τ_3 in either the high state (in-field loop) or the low state (remanent loop) conditions [117, 118]. The waveform of PFS is shown in Fig. 5b.

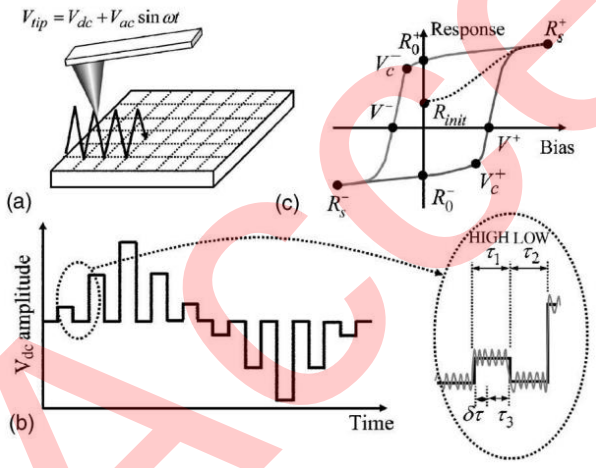

Fig. 5 Switching and driving waveforms of PFS: (a) electric signal supplied to the tip, (b) one cycle of the triangular square wave, and (c) a typical *PR* hysteresis loop. V^+ and V^- are forward and reverse coercive voltages. V_c^+ and V_c^- are forward and reverse nucleation voltages. R_s^+ and R_s^- are forward and reverse saturation polarization. R_0^+ and R_0^- are the forward and reverse remanent polarization. R_{init} is the initial response [119]. Reproduced with permission. Copyright (2006) AIP Publishing.

The response at DC-off pulses is used to calculate the remanent hysteresis loop. The piezoresponse (*PR*) is calculated by the relation of $PR = A\times\cos(\phi)$. A typical hysteresis loop of *PR* versus bias is shown in Fig. 5c. From this loop, many critical parameters describing the switching processes can be extracted and analyzed, including forward and reverse coercive biases (V^+ and V^-), remanent piezoresponses (R_s^+ and R_s^-), saturation piezoresponse (R_0^+ and R_0^-), nucleation bias (V_c^+ and V_c^-), and work of switching (defined as the area enclosed by the hysteresis loop).

4 Piezo-/ferroelectricity in protein-based biomaterials and implications

The reported piezoelectric coefficients of protein-based biomaterials differ over several orders of magnitude in the literature (Table 1) [6], which raises questions for scientists. A certain biomaterial should have the specific piezoelectric coefficients that are determined from a given molecular structure. Here we take collagen and elastin as representative examples and focus on the analysis of their molecular structure-property-functionality relations. Collagen and elastin are two types of proteins produced by fibroblasts that form the fibrous components of the connective tissues. Understanding the structure-property-functionality relations of biomaterials can fulfill the expectation of mimicking their properties in the design of innovative smart materials and devices [120].

4.1 Molecular structures of collagen and elastin

More than 16 types of collagens are in the human body (Table 2). 80-90 % of them fall into three categories: type-I, type-II, and type-III. These collagens are known as fibrous collagen because of their long strands [121]. Although their structures and the synthesizing processes are similar, they exist and function in different organs and tissues of the human body. Collagen type-I is abundant in bones, tendons, ligaments, skins, and teeth. Collagen type-II is abundant in the cartilages and eyes. Collagen type-III is abundant in the muscles, blood vessels, and skins. The collagen in bones is mainly composed of α chains, including α1 and α2 types of chains. These two types of chains are composed of amino acids, such as proline (Pro), glycine (Gly), valine (Val) and alanine (Ala), which are slightly different in amino acid composition and sequence [122]. Normal type-I collagen is a heterotrimer triple-helical molecule consisting of two α1 chains and one α2 chain [123]. An amino-terminal (N-terminal) and a carboxyl-terminal (C-terminal) locate at the two ends of the collagen molecule. The entire α chain consists of thousands of residues with repeated Gly-X-Y triplets, excluding the C-terminal and N-terminal sequences [124]. Fig. 6 illustrates the collagen peptide chain.

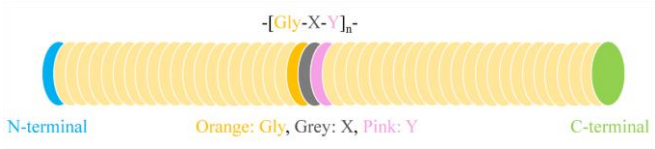

Fig. 6 A collagen peptide chain.

In the triple-helical region, the Gly-X-Y triplets are distributed periodically. The side chain of Gly, an H atom, is the only one that can fit into the crowded center of a three-strand helix. Hydrogen bonds link the peptide bond N-H of a Gly residue with a peptide carbonyl (C=O) group in an adjacent polypeptide to hold the three chains together. The fixed angle of the C-N peptidyl-Pro or peptidyl-Hyp bond enables each polypeptide chain to fold into a single helix with a geometry that three polypeptide chains can twist together to form a three-strand helix. Many three-strand type-I collagen molecules pack together side-by-side, forming fibrils with a diameter of 50-200 nm. In fibrils, adjacent collagen molecules are displaced from one another by 67 nm along the axial axis, about one-quarter of their length. Each collagen molecule has polar bonds, characterized by N and C terminals, resulting in a dipole moment (or polarization) along the axial axis of the molecule, which is directed from N to C termini [125]. Fig. 7 illustrates the molecular structure and the organization of type-I collagen. The type-I collagen has a crucial role in maintaining the structural integrity and functional properties of organs and tissues [126, 127].

Table 1. Piezoelectricity in selected protein-based biomaterials from the literature [6].

Coefficient	Source	Preparation	Piezoelectric coefficient
Longitudinal (d_{33})	silk	simple cut	0.023 pm/V
	wool	simple cut	0.0033 pm/V
	horse femur	simple cut	0.0033 pm/V
	horse achilles tendon	simple cut	0.066 pm/V
	human bone	simple cut	7−9 pC/N
	spider silk	embedded in PDMS	0.36 pm/V
	fish swim bladder		22 pC/N
	porcine thoracic aorta	purified elastin fiber	0.75 pm/V
Transverse (d_{31})	silk	simple cut	0.02 pm/V
	wool	simple cut	0.01 pm/V
	horse femur	simple cut	0.0033 pm/V
	horse achilles tendon	simple cut	0.013 pm/V
	human cornea	diagonal cut	2250 pC/N
		vertical cut	600 pC/N
		horizontal cut	200 pC/N
Shear (d_{14}= -d_{25})	human bone	simple cut	0.12 pC/N,
		simple cut	0.12 pm/V
	silk	simple cut	−1.09 pm/V
	wool	simple cut	−0.066 pm/V
	horse femur	simple cut	−0.21 pm/V
	horse achilles tendon	simple cut	−1.9 pm/V
	silk	mechanical stretching by 18 zone drawing (heating)	−0.7 pC/N
		methanol-wet drawing	−0.4 pC/N
		water-wet drawing	−0.05 pC/N
	skin	simple cut	0.2 pC/N
	wool	simple cut	0.1 pC/N
	horn	simple cut	1.8 pC/N
Shear (d_{15})	animal cortical bone	simple cut	0.1−0.3 pm/V
	collagen fibril	collagen fibril on a gold substrate	1 pm/V
	bovine achilles tendon	collagen nano-fibril	2 pm/V

Table 2 Different types of collagens.

DISTRIBUTION	TYPE	MOLECULAR FORMULA	OLYMERIZED FORM	TISSUE
Fibril-forming (fibrillary)	I	[α1(I)]2α2(I)	Fibril	Bone, skin, tendons, ligaments, cornea, internal organs (accounts for 90 % of body collagen)
	II	[α1(II)]3	Fibril	Cartilage, invertebral disc, notochord, vitreous humor of the eye
	III	[α1(III)]3	Fibril	Skin, blood vessels, internal organs
	V	[α1(V)]2α2(V) and α1(V)α2(V)α3(V)	Fibril (with type-I)	As for type-I
	XI	[α1(XI)α2(XI)α3(XI)	Fibril (with type-II)	As for type-II
Fibril-associated	IX	[α1(IX)α2(IX)α3(IX)	Lateral association with type-II fibrils	Cartilage
	XII	[α1(XII)]3	Lateral association with some type-I fibrils	Tendons, ligaments, some other tissues
Network-forming	IV	[α1(IV)]2α2(IV)	Sheetlike network	Basal lamina
	VII	[α1(VII)]3	Anchoring fibrils	Beneath stratified squamous epithelia
Transmembrane	XVII	[α1(XVII)]3	Not known	Hemidesmosomes
Others	XVIII	[α1(XVIII)]3	Not known	Basal lamina around blood vessels

Different from the structural proteins, elastin forms the fabric of stretchable tissues, such as skins, blood vessels, and elastic ligaments [128]. It provides the elasticity re-

quired for physiological activity. For example, in the walls of the aorta, collagen provides the strength required to prevent rupture due to high blood pressure, while the elastin is also responsible for resilience and extensibility of the aorta by impartation, minimizing the energetic demands on the heart, and to ensure smooth blood flow to different organs in the entire human body [129, 130]. About 80% of the sequence of tropoelastin consists of repeated motifs of Pro-Gly-Val-Gly-Val-Ala, Pro-Gly-Val or Pro-Gly-Val-Gly-Val. Models of elastin structures and functions reported in the literature are simplistic and with large discrepancies. Urry *et al.* proposed a β-spiral model, in which elastin had an ordered spiral [131]. Flory *et al.* suggested a random, rubber-like, highly disordered structure of elastin, which changed the ordered spiral to a predominantly random coil [132, 133]. Rauscher *et al.* obtained a disordered conformational ensemble for the elastin-like peptide $(Gly\text{-}Val\text{-}Pro\text{-}Gly\text{-}Val)_7$, which was a heterogeneous ensemble of conformations (Fig. 8) [134, 135]. These structures are not random coils and contain no α-helix or extended β-sheet (secondary structures of a polypeptide chain). They are disordered but not random [136]. Fig. 8b shows the 16 unique configurations of an elastin-like peptide monomer.

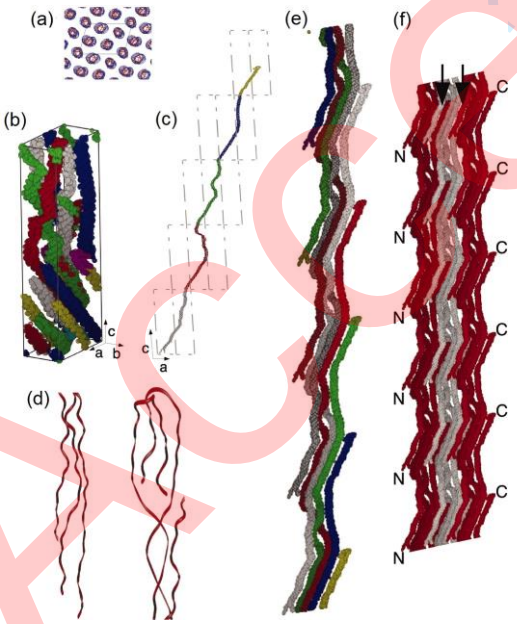

Fig. 7 The illustration of collagen organization and structure. (a) The quasi-hexagonal packing of the molecular segments; (b) C^{α} carbons rendered as line spheroids showing the conformation of the staggered collagen segments within a unit cell (cell axis shown); (c) molecular path of a collagen molecule through successive unit cells in the a-c plane; (d) enlarged view of the telopeptides of type-I collagen at the bottom of (c); (e) several staggered collagen molecules with right-handed twist; (f) Three microfibrils are shown side by side to indicate the probable binding relationship. The N-terminal and C-terminal are shown [127]. Reproduced with permission. Copyright 2006, National Academy of Sciences.

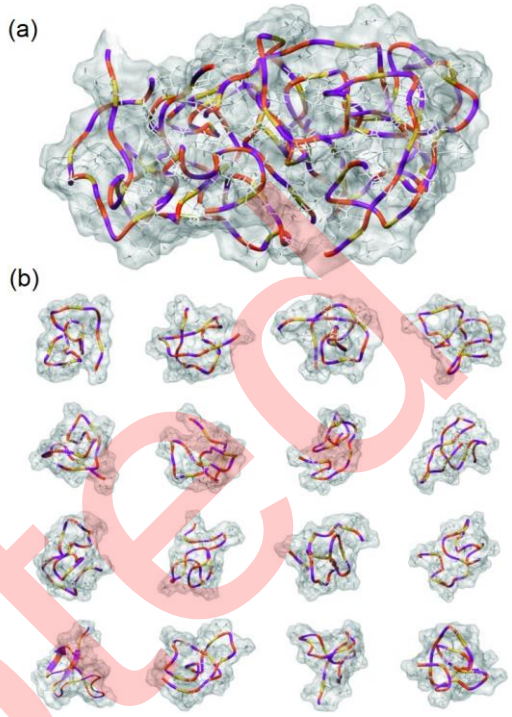

Fig. 8 Configurations of the elastin-like peptide $(Gly\text{-}Val\text{-}Pro\text{-}Gly\text{-}Val)_7$. (a) An aggregate of 8 chains; (b) 16 unique configurations of a monomer [136]. Reproduced with permission. Copyright 2012, Springer.

4.2 Electromechanical coupling in collagen and elastin

Fukada reported that collagen was piezoelectric with shear piezoelectric coefficient ranging from 0.2 to 2.0 pC/N [62]. Collagen can exhibit different structural organizations, thus complicating the determination of the origin of its piezoelectricity. Marino *et al.* found that the electrodeposited collagen films were more organized and with higher piezoelectric responses than those of the evaporated films. They suggested that the piezoelectricity originated from the tropocollagen molecule or aggregated structures with less than 50 Å diameter [137]. The emergence of PFM and spectroscopy have successfully provided access to the nanoscale inspection of the piezoelectric response of biomolecules. Theoretically, it considers the inhomogeneity of the electric field under the probe apex and screening effects of the applied electric field to obtain the piezoelectric coefficients of materials. Minary-Jolandan *et al.* applied the lateral PFM (LPFM) to probe the shear piezoelectricity in bone with high resolution down to the sub-fibrillar structure of individual collagen fibril (Fig. 9) [84]. The shear piezoelectricity maps of collagen fibrils exhibited heterogeneous structures. Individual collagen fibril showed a periodic pattern with a D-space of 60-70 nm. They believed that the heterogeneity in piezoelectricity maps of collagen fibril might be relevant to the modulation of the ionic environment of bone and might have effects on the bone mineralization process. Denning *et al.* measured the structure and piezoelectric property of the aligned collagen membranes using LPFM

under ambient conditions. They demonstrated that the piezoelectricity of the collagen membrane was an order of magnitude lower than that of collagen fibril in rat tail tendon. They believed the lower response of collagen membranes was attributed to less-ordered molecular assembly than the periodic D-space structure in collagen fibrils [138]. Although the piezoelectricity could be aroused from collagen structures, supramolecular interaction could also lead to the piezoelectric behavior of collagen. For example, Sousa Neto *et al.* did studies on collagen membranes with iron as impurities. They found that doping the iron in the collagen structure could increase the value of piezoelectric strain tensor element d_{14} [139]. Besides, hydrated proteins were reported polarizable in reference [107, 140] from which we might expect similar phenomena exhibited by the collagen-water system. However, the ferroelectricity of collagen has not been observed yet.

As the key extracellular matrix (ECM) protein found in all connective tissues of vertebrates [141, 142], elastin was found to exhibit polarization switching behavior by SSPFM and confirmed to be ferroelectric by macroscopic pyroelectric measurements [64]. The polarization of elastin was intrinsic in tropoelastin at the monomer level, resembling the unit cell of classical perovskite ferroelectrics. Fig. 10 shows the responses of tropoelastin monomers characterized by PFM and SSPFM. The PFM response vs. voltage curve shows a bilinear relationship (Fig. 10a). The PFM phase (Fig. 10b) and amplitude (Fig. 10c) reveal the piezoelectricity of tropoelastin. The switching spectroscopy maps reveal consistent polarization switching (Fig. 10d). The phase and amplitude butterfly loops (Fig. 10e and f) were recorded at three different locations. Although elastin was confirmed to be ferroelectric, it was only found in the arteries of vertebrates. The existence of ferroelectricity in other protein-based biomaterials has remained a puzzle. For example, the fibril-forming type-I collagen appeared to be non-switchable [143], whereas it is rich in amino acids such as glycine and proline. Another point worthy of noting is that the conformational disorder is a constitutive feature of elastin structure and function. However, collagen has shown a highly ordered triple helical structure [134, 144, 145]. Therefore, elastin is more flexible and easily stretched. The bioferroelectricity is supposed to be related to the degree of structural ordering.

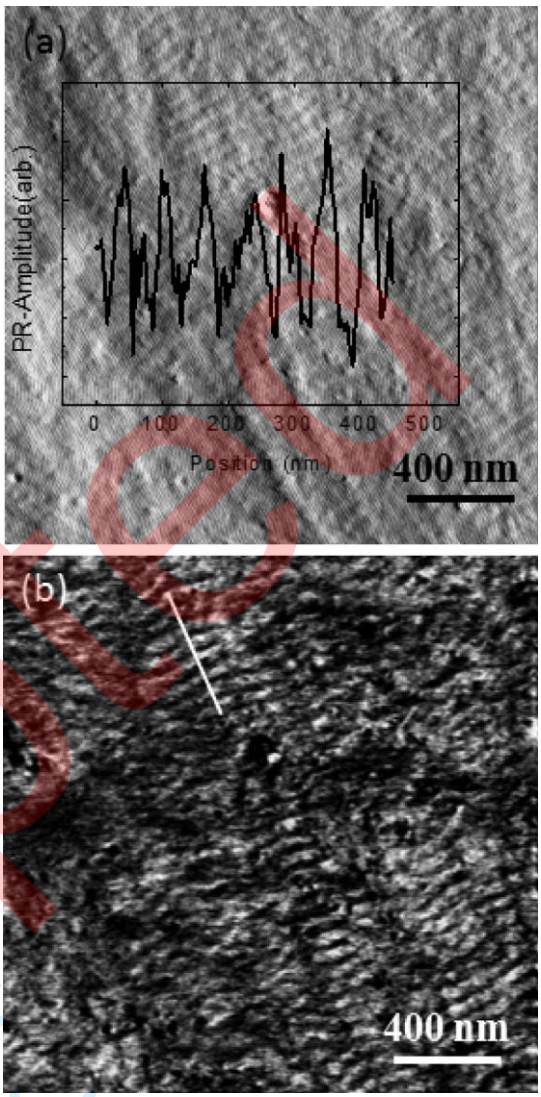

Fig. 9 The shear piezoresponse in cortical bone measured by LPFM. (a) AFM deflection image, and (b) the lateral PFM response [84]. Reproduced with permission. Copyright (2010) AIP Publishing.

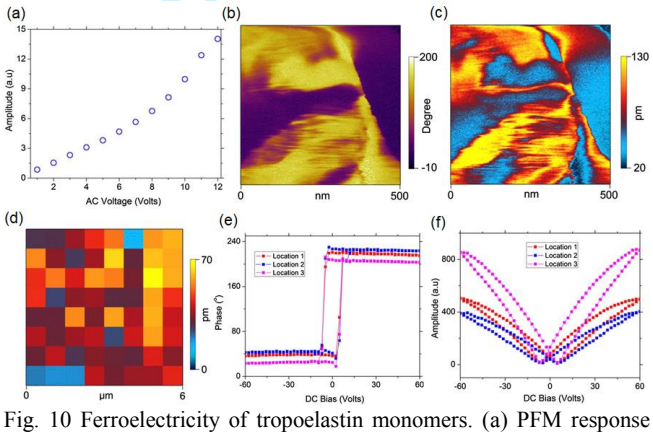

Fig. 10 Ferroelectricity of tropoelastin monomers. (a) PFM response vs. AC voltage; (b) PFM phase and (c) amplitude images; (d) SSPFM image at zero DC voltage; (e) phase hysteresis and (f) butterfly loops of three representative points [64]. Reproduced with permission. Copyright (2014) National Academy of Sciences.

The piezoelectric properties of collagen and elastin are convincible because they are formed by amino acids, among which 21 amino acid molecules are non-centrosymmetric, and 20 of them show piezoelectricity [125]. The situation can be generalized to other protein-based biomaterials. However, the bioferroelectricity should be carefully proclaimed with a good cognition of the structure-property-functionality relation and a systematic verification method. The structural and conformation changes arouse various biological functions. Moreover, the nanoscale experiments by using PFM and related spectroscopy techniques are usually coupled with non-piezoelectric EM coupling effects so that the measured piezoelectricity should be carefully evaluated. In the next section, we will discuss other factors that can cause EM signals in experiments.

5 Identification of intrinsic piezoelectricity in biological materials

Since other forms of EM couplings (electrostriction and flexoelectricity) and experimental factor (electrostatic effects) may contribute to the overall EM signals detected by PFM, it is quite essential to differentiate them from the intrinsic piezoelectricity. In this section, we review the influences of electrostriction, flexoelectricity, and experimental electrostatic effect on the measured piezoelectric phenomena.

5.1 Other types of EM couplings

Both the electrostriction and flexoelectricity may contribute to the measured EM response. Electrostriction indicates that the dielectric material displays deformation under an applied electric field. It does not require electric dipoles in the dielectric materials (Fig. 11a). Theoretically, all polarizable materials can show electrostriction behaviors [146]. Electrostriction has a quadratic relationship between the mechanical strain and the electric field (Equation 3). Using the third derivative of the Gibbs free energy G (Equation 4), the direct electrostrictive (M^{d}_{ijkl}) and converse electrostrictive (M^{c}_{ijkl}) coefficients are found to be equal and can be determined from the Maxell relationship (Equation 5):

$$dG = -S \cdot dT - \varepsilon_{ij} \cdot d\sigma_{ij} - P_k \cdot dE_k \quad (4)$$

$$M^{d}_{ijkl} = -\left(\frac{\partial^3 G}{\partial \sigma_{ij} \partial E_k \partial E_l}\right) = \left(\frac{\partial^2 \varepsilon_{ij}}{\partial E_k \partial E_l}\right) = -\left(\frac{\partial^3 G}{\partial E_k \partial E_l \partial \sigma_{ij}}\right) = \left(\frac{\partial \chi_{kl}}{\partial \sigma_{ij}}\right) = M^{c}_{ijkl} \quad (5)$$

where S, T, and σ are the entropy, temperature, and stress, respectively.

Flexoelectricity is defined as a dielectric material that exhibit a spontaneous polarization induced by a strain gradient. Fig. 11b illustrates the flexoelectric effect. It describes that a dielectric material can deform under a strain or stress gradient generated in the material. The gradient breaks the inversion symmetry of the material, leading to nonuniform displacements of atoms [147-149]. The flexoelectric effect usually is small, but it may dominate on the nanoscale. Therefore, the measured piezoelectricity can be veiled by flexoelectricity in PFM measurements. Flexoelectricity has been reported to be associated with many biomechanical phenomena such as hair cells to amplify sound [150] and embedded proteins in biomembranes to act as mechanical motors [151]. Together with the direct piezoelectricity, the total electric polarization upon mechanical deformation of a solid can be written as:

$$P_k = d_{kij}\sigma_{ij} + \mu_{kijl}\frac{\partial \varepsilon_{ij}}{\partial x_l} \quad (6)$$

where d_{kij}, σ_{ij}, μ_{kijl}, ε_{ij}, and x_l are the piezoelectric constant, stress, flexoelectric coefficient, strain, and position coordinate, respectively [152-154]. The d is zero for all groups containing inversion symmetry. Therefore, the flexoelectric effect can exist in all the 32 point groups [155] since the inversion symmetry is disrupted by strain gradient [7]. In centrosymmetric materials, Equation 6 can be written as:

$$P_k = \mu_{kijl}\frac{\partial \varepsilon_{ij}}{\partial x_l} \quad (7)$$

Tagantsev reported that the flexoelectric coefficient could be scaled with the dielectric susceptibility of the material, which can be expressed as [156, 157]:

$$\mu = \chi\gamma\left(\frac{e}{a}\right) \quad (8)$$

where γ, e and a are the materials parameter constant, electron charge and lattice constant, respectively. In the expression above, there are several factors that contributed to the polarization, including static bulk flexoelectricity, dynamic bulk flexoelectricity, and surface flexoelectricity.

The converse flexoelectric effect can be described as the linear coupling between the induced elastic stress and the electric field gradient:

$$T = \mu\frac{\partial E}{\partial x} \quad (9)$$

where T is the induced elastic stress.

Electrostriction, flexoelectricity, and piezoelectricity are usually coupled with one another. They have the same correlated parameters, including stress, strain, polarization, and electric field. For example, both piezoelectricity and electrostriction indicate the mechanical strain induced by an applied electric field. Therefore, the piezoelectric and electrostrictive polarizations are mixed in the measurement of strain under an electric field. In addition, the direct piezoelectric polarization can be mixed with flexoelectric polari-

zation when applied mechanical stress that generates nonuniform strain inside materials [6]. However, there are differences in these effects. The electrostrictive strain is proportional to the square of electric polarization (Equation 3) so that the reverse of the electric field will not change the strain. However, the piezoelectric strain is linearly proportional to electric polarization (Equation 3), so the strain is affected by the reverse of the electric field. Moreover, piezoelectricity refers to polarization due to uniform strain, while flexoelectricity refers to polarization due to strain gradient (Equation 6). Piezoelectricity changes sign under space inversion, while flexoelectricity is insensitive to the space inversion [158]. Therefore, checking the point groups is a good way to distinguish piezoelectricity. Besides, flexoelectricity is size-dependent [159, 160], hence possibly increasing the length scale is beneficial to differentiate the flexoelectricity from piezoelectricity.

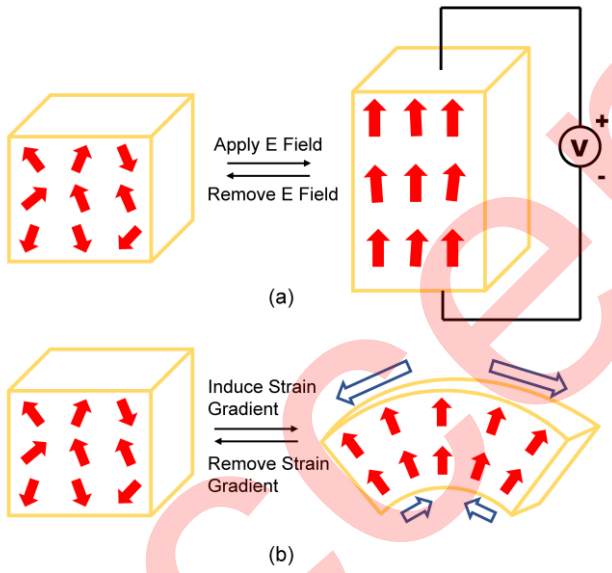

Fig. 11 Illustration of (a) electrostriction and (b) flexoelectricity [6]. Reproduced with permission. Copyright (2018) ACS Publications.

5.2 Experimental factor

The electrostatic effect is a parasitic interaction between the conductive AFM tip/cantilever and the sample surface, regardless of the operational modes (i.e., contact or non-contact modes), which originates essentially from the Coulombic electrostatic force. The Coulombic force between separated charges can cause deformation of the material, as shown in Fig. 12. When the sample with two electrodes is connected to an external voltage, the electrostatic force is generated between the oppositely charged surfaces, which can lead to the compression of the sample in the thickness direction and the expansion in the planar direction [16]. In the nanostructured compliant biomaterial, there may exist a large electric potential between the sample and electrodes, as well as the sample surface and internal atoms. The electrostatic effect could contribute significantly to the measured EM signals, making it difficult to identify the true piezoelectric response [99, 100]. However, there are some methods to identify the electrostatic effect experimentally, which are discussed in the next section.

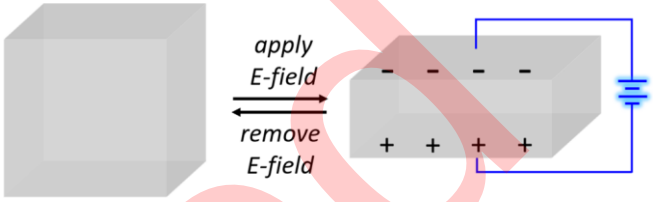

Fig. 12 Illustration of the electrostatic effect [6]. Reproduced with permission. Copyright (2018) ACS Publications.

6 Piezoresponse force microscopy and spectroscopy

In this section, we will review the approaches for identifying the piezoelectric contribution from the measured EM signals in PFM and related techniques.

6.1 Electrostatic effect in measurements

When conducting the PFM experiments, the EM phase signal of each domain is proportional to that of the electrostatic phase. Gómez *et al.* gave a theoretical description of the total phase difference versus the electrostatic phase with different ratios of A_{Elec}/A_{Piezo} (Fig. 13) [161]. They found that when the electrostatic effect was quite low (A_{Elec}/A_{Piezo} = 0.001), the phase difference of domains equaled to 180°, indicating that the measured signal mainly comes from the piezoresponse. When the electrostatic effect was increased (A_{Elec}/A_{Piezo} = 0.5), the measured EM phase was 126°. When the phase difference decreased up to a point (A_{Elec}/A_{Piezo} = 2), all the phase recorded was directly proportional to the electrostatic effect and independent of the piezoelectric effect [161].

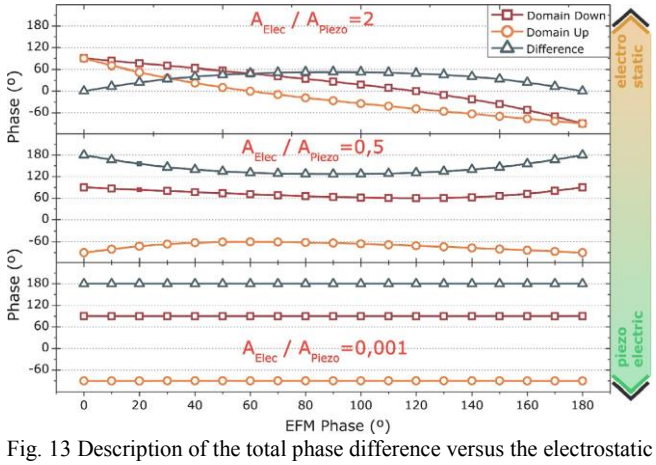

Fig. 13 Description of the total phase difference versus the electrostatic

phase with different ratios of A_{Elec}/A_{Piezo}. When the ratio is 0.001, the phase difference is independent of the electrostatic signal. The phase of each domain decreases as the ratio increases, up to the point that all the phase recorded is proportional to the electrostatic signal and independent of the piezoelectric signal [161]. Reprinted with permission. Copyright (2018) Elsevier.

Gómez *et al.* also suggested that the electrostatic effects could be diminished by using longer ultra-stiff tips [161]. They developed a theory that could decouple the effects of electrostatic contribution in the total cantilever vibration and addressed the problem through using longer ultra-stiff probes, which provided high sensitivity, allowed lowest electrostatic interaction, and avoided working in high-frequency regime. They tested the theory by conducting PFM on a periodically poled lithium niobate (PPLN) crystal, which showed well-defined 0° and 180° domains (Fig. 14). It was found that both soft diamond and platinum tips were quite sensitive to DC bias, while longer ultra-stiff tips were independent of DC bias.

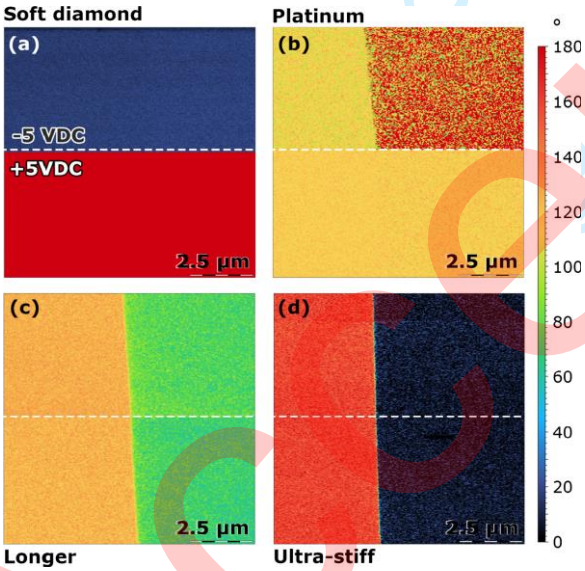

Fig. 14 PFM phase image by (a) a soft diamond-coated probe, (b) a standard platinum-coated tip, (c) a longer tip length probe and (d) an ultra-stiff probe with voltage (5 V_{AC}, 105 kHz, +5 V_{DC}) applied to the sample from bottom to the middle. The voltage -5 V_{DC} is applied from middle to bottom [161]. Reproduced with permission. Copyright (2018) Elsevier.

Balke *et al.* demonstrated a cantilever-resonance-based method to quantify the electrostatic forces on a probe arising from a surface potential or when a bias voltage was applied to the AFM probe [162]. They showed that the local topography had a direct effect on the electrostatic forces acting on the tip apex, and the electrostatic force strongly depended on the tip apex shape. In combination with modeling, they analyzed the cantilever vibration at its resonance in response to a harmonic force $F_{apex}\cdot\sin(\omega t)$ applied to the tip apex along the normal to the sample surface. The amplitude of the tip apex displacement induced by the harmonic electrostatic force at the tip apex was obtained. Fig. 15 shows the calculated electrostatic force linear density.

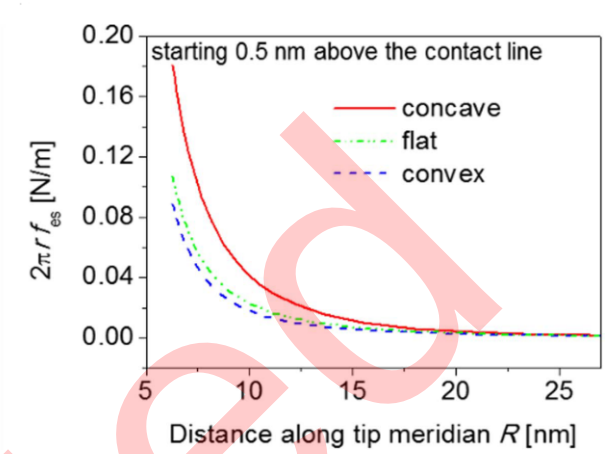

Fig. 15 Calculated electrostatic force linear density $2\pi r\cdot f_{es}$ (R) along the tip meridian for the concave, flat, and convex sample surfaces for the same conditions [162]. Reproduced with permission. Copyright (2017) IOP Publishing.

It is worthy of noting that using ultra-stiff probes to reduce the electrostatic effect is suitable for materials of which the elastic moduli are significantly higher than that of the probe. However, such a method encounters problems for organic polymers and biomaterials (Young's modulus of the material is small comparing to the probe), in which the electrostatic responses are quite large. Besides, an ultra-stiff probe can cause significant deformation of the soft biomaterial. The mismatch between the soft surface and stiff AFM probe leads to a small amplitude response even under large applied electric field and small signal to noise ratio in the prevalent dual AC resonance tracking (DART) PFM technique [163] which uses contact resonance for signal enhancement [164]. Marvin *et al.* changed the thicknesses (Δt) of short peptides, peptoids, and control small molecule dodecanethiol (DDT) films over a series of applied voltages (1.5-4 V) averaged across specific areas. They calculated the slopes from a linear fit to plots of Δt vs. applied voltage to derive the piezoelectric responses of these materials along the polarization axis (d_{33}). The non-zero intercepts of the lines were due to electrostatic and tip-sample interactions (Fig. 16) [165]. They demonstrated the validity of their method by successful determination of the piezoresponse of quartz.

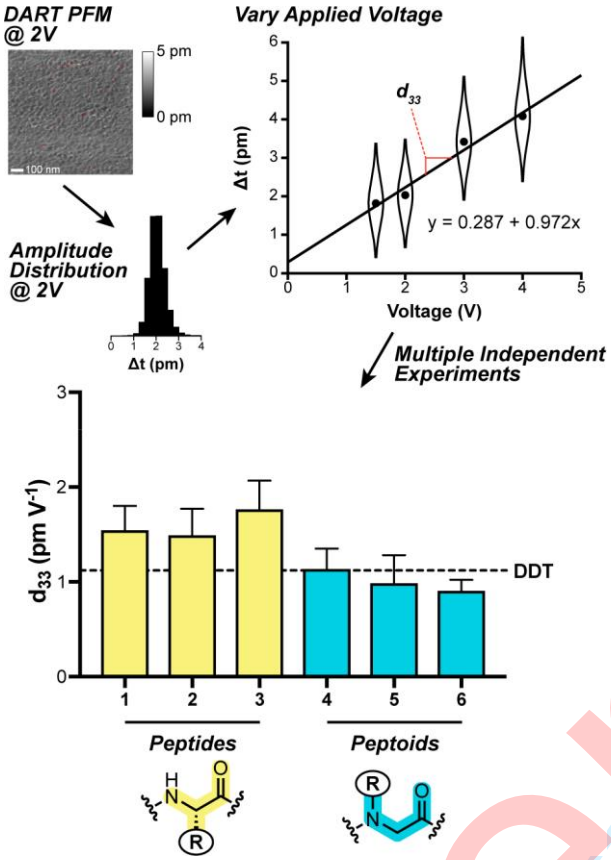

Fig. 16 Summary of DART-PFM method used to determine piezoelectric responses and d_{33} values obtained from replicate independent experiments on peptides (1-3), peptoids (4-6), and dodecanethiol (DDT) [165]. Reproduced with permission. Copyright (2017) ACS Publications.

6.2 Electrostriction and flexoelectricity in measurements

Eliseev *et al.* theoretically demonstrated the contribution of electrostriction could not be readily separated from the PFM response [166]. In particular, the electrostriction became significant for materials with low dielectric constants. Seol *et al.* adopted the finite element method to simulate the cylindrical geometry with the axially symmetric tip at various frequencies [167]. They calculated the electrostrictive contribution to the EM amplitudes, as shown in Fig. 17. The frequency-dependent amplitude was found to increase as the frequency decreased. In addition, they proved that by sweeping the frequency-dependent AC amplitude, it could be able to extract the ferroelectric effect.

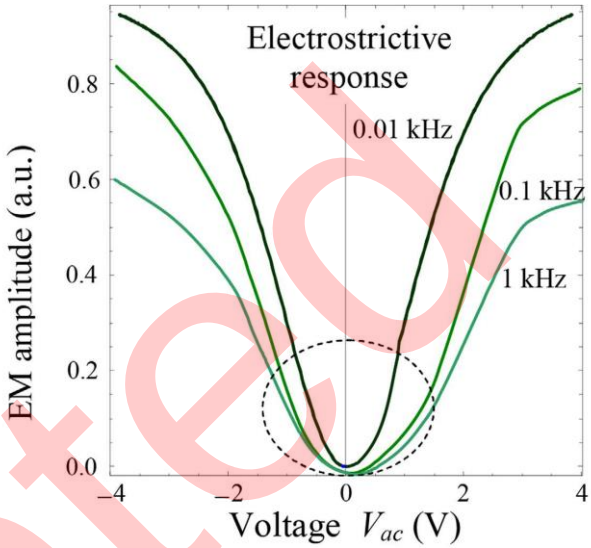

Fig. 17 The influence of electrostrictive response on the EM response measured at different frequencies (0.01 kHz, 0.1 kHz, and 1 kHz) [167]. Reproduced with permission. Copyright (2016) Nature Publishing Group.

Chen and Li *et al.* compared the first and second harmonic responses under vertical strain-based SPM of lead zirconate titanate (PZT) thin film, lithium iron phosphate (LFP) thin film, and soda-lime glass. They found that the three materials had quite distinctive responses, as shown in Fig. 18 [168]. For the piezoelectric PZT thin film, the response was predominantly linear to the AC electric field, indicating the measured response was mainly due to the piezoelectricity (according to Equation 3). For the LFP thin film, there was a significant quadratic strain because of electrostriction (according to Equation 3), though the second harmonic response was slightly smaller than the first harmonic one. For the glass, the second harmonic response was slightly higher, suggesting a substantial quadratic contribution to the measured strain.

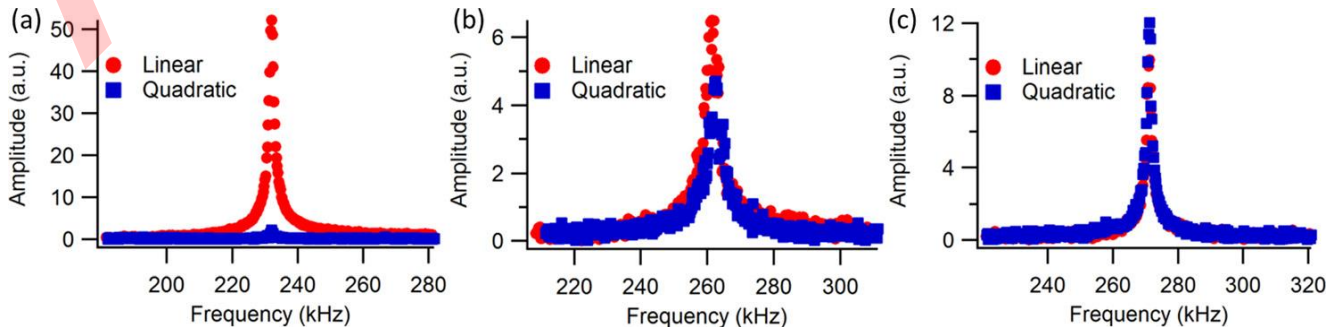

Fig. 18 First and second harmonic responses under vertical strain-based SPM of (a) PZT; (b) LFP; and (c) soda-lime glass. Reproduced with per-

mission [168]. Copyright (2014) AIP Publishing.

The flexoelectric effect becomes significant in thin films and nanostructures and is reported as the key EM effect for important biomechanical phenomena [7]. In addition, the flexoelectric effect could affect the ferroelectric properties of materials, including their critical thickness, electrical transport of the domain wall, and polarization switching [94, 169]. Both the piezoelectricity and flexoelectricity describe the linear EM effect [170]. The coupling effect of flexoelectricity and piezoelectricity in piezoelectric nanostructures has not been completely clarified yet, not to mention the thin and nanostructured biomaterials. Kalinin *et al.* explored the EM phenomenon in tobacco mosaic viruses (TMV) by using PFM. They found that in the small-sized and highly symmetric materials, the flexoelectric effect dominated the observed EM behavior. Fig. 19 shows the results of TMV. They estimated the relative contributions of the piezoelectric and flexoelectric responses to the measured PFM signal using piezoelectric and flexoelectric models, and they found that the linear behavior in Fig. 19c should be explained by the flexoelectric effect instead of the piezoelectric effect [171].

Zhang *et al.* adopted AFM to investigate the deformation of human embryonic kidney (HEK 293) cells upon voltage changes of a stimulus-evoked membrane (Fig. 20a). It was found that the cells swelled when depolarization (hyperpolarization) happened because a 100 mV depolarization of the cell membrane caused approximately 0.6 nm of swelling (Fig. 20b). To understand the observation, they developed a model (Via the Lippmann relation) to explain the voltage induced movement of the membrane. The model showed a dependence of tension on the membrane voltage so that the membrane should change the cellular radius. The observation resembled the converse flexoelectricity [172].

The above works are associated with math models, which are important for the studies of piezoelectric and flexoelectric coupling effects. The researches in the field are still growing [173-176].

7 Discussion and perspectives

For biological materials and systems, their hierarchical self-assembly structures usually involve different order parameters spanning multiple length scales and thus have made them far from good-fetched. For protein-based materials, different biomacromolecules, peptides, and proteins may exhibit distinct properties even though all of them are built up by known amino acids. Biopiezo-/bioferroelectricity should be carefully proclaimed after clarifying the structure-property-functionality relation. Since the bio-functions originate from small length scales, i.e., atomic- or nanoscale level, the advanced SPM techniques combing with spectroscopy offer effective ways to explore the mechanisms behind the novel biopiezo-/ferroelectric phenomena. However, caution should be paid to the influences of other types of EM couplings and factors aroused from SPM experimental measurements. The decoupling of various EM responses is still a hot research topic, and we expect more innovative and fruitful works in the future.

On the other hand, the biopiezo-/ferroelectricity holds great potentials for in vivo sensing, drug delivery, and tissue reconstruction, especially the piezoelectric response arising from strong supramolecular dipoles in biomaterials and systems, which can be tuned by molecular chemistry and packing. It has opened new opportunities for the realization of functional devices. Also, the molecular/supramolecular interactions in the ordered structure may have more than two stable states. It means that the multiple orthogonal supramolecular interactions in molecular materials can lead to multiple supramolecular dipoles in the ordered structure, offering the essential conditions for the realization of molecular ferroelectrics with better storage capacity. For example, Tayi and co-workers reported the supramolecular charge-transfer networks, which showed ferroelectric polarization switching above the room temperature (Fig. 21). These switchable polarization networks consist of hydrogen-bond networks and charge-transfer complexation of donor and acceptor molecules in a mixed stack [177]. The combination of hydrogen-bond and charge-transfer complexation interactions has promoted promising supramolecular organic devices. Such situations can be expected for biobased devices because hydrogen-bond and charge-transfer complexation are also commonly interactions in biomaterials and systems.

With the fast development of high-performance computing methods, researches on the piezo-/ferroelectric properties of biomaterials and biomolecules have been facilitated by using quantum mechanical calculations, which can be used to predict the full piezoelectric tensor of biomolecular crystals, including amino acids and small peptides [102]. For example, the density functional perturbation theory (DFPT) can be used to understand inside the peptide structures for the desired EM properties. The simulation methods can advance the experiments and allow insight into the evolution of conformational and hierarchical structure changes in biological materials that originate from highly piezoelectric building blocks. In addition, the research frontier, such as deep learning, shows abilities to predict the protein crystal growth, peptide evolution, structure-based rational drug design, and device fabrication, thus guiding the experimental studies and promoting the developments of biobased devices.

8 Summary and conclusions

Although piezoelectricity of amino acids is surely accepted,

particularly, the glycine and lysine show the highest piezoelectric responses and are promising for engineering highly piezoelectric peptides in the future, it is unrealistic to consider the piezoelectricity in the peptides or the protein-based materials regardless of their structures and conformations. Elastin and collagen are good examples that own different molecular structures, thus function differently in the body. In terms of bioferroelectricity, it should be carefully proclaimed due to the lack of macroscopic experiments confirmation. The observed EM coupling signals measured by PFM and spectroscopy are usually associated with piezoresponse, flexoelectricity, electrostriction and electrostatic effects, and some others. In literature, many researchers have proposed methods to extract the piezoresponse or minimize the perturbance factors. Nevertheless, combing the multiple nanoscopic and macroscopic experimental techniques, as well as the simulation, is the most persuasive approaching method. Physiological and pathological significances of biopiezo-/bioferroelectricity remain to be largely explored, but we expect more exciting discoveries.

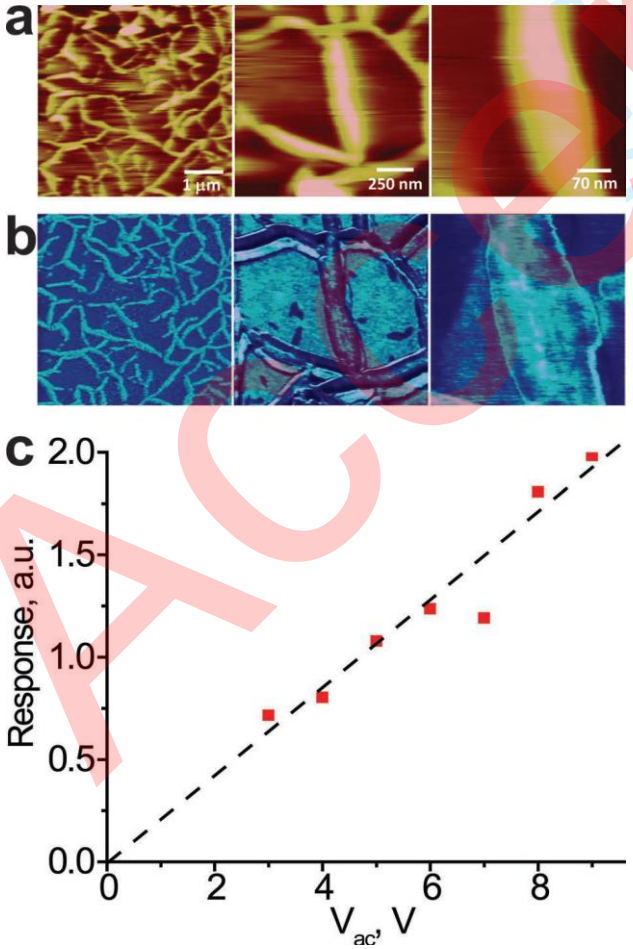

Fig. 19 Flexoelectricity in the tobacco mosaic virus (TMV). (a) Morphology of TMV at different size scales; (b) PFM deformation images of TMV associated with the morphology images; (c) the EM response of TMV under an applied AC voltage with varying amplitude. Reproduced with permission [171]. Copyright 2006, American Institute of Physics.

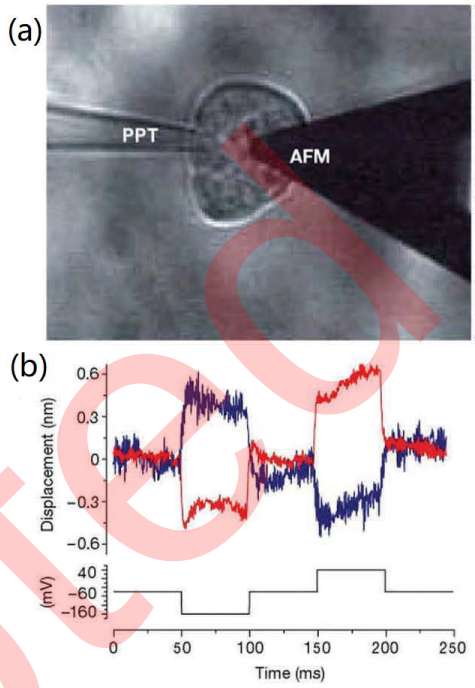

Fig. 20 Flexoelectric behavior of cellular membranes. (a) Micrograph of a cell which is voltage-clamped and probed with an AFM cantilever. The pipette (PPT) can be seen; (b) Cell movements driven by ±100 mV voltage pulses from a holding potential of -60 mV at normal (blue trace) and nominal 0 mM (red trace) ionic strengths. The positive displacement indicates the cantilever moving into the cell [172]. Reproduced with permission. Copyright 2001, Nature Publishing Group.

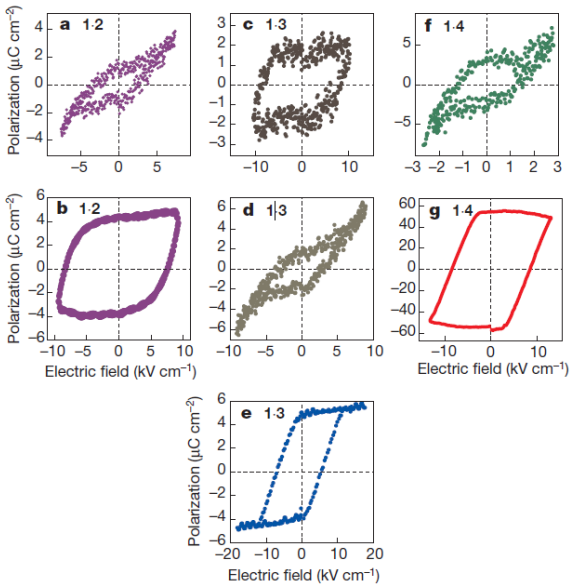

Fig. 21 Macroscopic ferroelectric hysteresis loops in supramolecular networks. Polarization versus electric field curves for lock arm supramolecular ordering (LASO) complexes. (a, b) complex of 1 and 2; (c-e) complex of 1 and 3; and (f, g) complex of 1 and 4 measured at various temperatures: (a) 300K, (b) 74K, (c, d) 300K and (e) 7K, (f) 300K and (g) 7K. Room-temperature hysteresis curves for LASO complexes are under-polarized because of leakage currents at high voltage. 1 is py-

romellitic diimide-based acceptor, while 2, 3, and 4 are derivatives of naphthalene, pyrene, and TTF, respectively [177]. Reproduced with permission. Copyright 2012, Nature Publishing Group.

This work was supported by the Ministry of Education (Singapore) through the National University of Singapore under the Academic Research Grant (ACRF) R-265-000-495-112 and R-265-000-596-112. The authors also would like to thank the financial support from the National Key Research and Development Program of China under the Grant No. of 2018YFB0407600, 2017YFA0206202, 2016YFA0300702, National Natural Science Foundation of China (Grant No. 51802250) and Key Research and Development Program of Shaanxi (Grant No. 2019TSLGY08-04). All researchers working on biopiezo-/bioferroelectricity and EM couplings are acknowledged, and we are regretful for not being able to summarize all the progress in this short review.

9 References

[1] P. X. Gao, J. Song, J. Liu, and Z. L. Wang, Adv. Mater. **19**, 67 (2007).
[2] Y. -B. He, G. -R. Li, Z. -L. Wang, C. -Y. Su, and Y. -X. Tong, Energ. Environ. Sci. **4**, 1288 (2011).
[3] J. Sirohi, and I. Chopra, J. Intell. Material Syst. Struct. **11**, 246 (2000).
[4] N. Amdursky, M. Molotskii, D. Aronov, L. Adler-Abramovich, E. Gazit, and G. Rosenman, Nano Lett. **9**, 3111 (2009).
[5] J. P. Hill, L. K. Shrestha, S. Ishihara, Q. Ji, and K. Ariga, Molecules **19**, 8589 (2014).
[6] I. Chae, C.K. Jeong, Z. Ounaies, and S. H. Kim, ACS Appl. Bio Mater. **1**, 936 (2018).
[7] T. D. Nguyen, S. Mao, Y. -W. Yeh, P. K. Purohit, and M. C. McAlpine, Adv. Mater. **25**, 946 (2013).
[8] P. V. Yudin, and A. K. Tagantsev, Nanotechnology **24**, 432001 (2013).
[9] J. Zhang, C. Wang, and C. Bowen, Nanoscale **6**, 13314 (2014).
[10] R. E. Newnham, V. Sundar, R. Yimnirun, J. Su, and Q. M. Zhang, J. Phys. Chem. B **101**, 10141 (1997).
[11] V. S. Bystrov, I. K. Bdikin, A. Heredia, R. C. Pullar, E. D. Mishina, A. S. Sigov, and A. L. Kholkin, in *Piezoelectric Nanomaterials for Biomedical Applications*, edited by G. Ciofani, and A. Menciassi (Springer Berlin Heidelberg, Berlin, Heidelberg, 2012), pp. 187-211.
[12] D. Seol, B. Kim, and Y. Kim, Curr. Appl. Phys. **17**, 661 (2017).
[13] B. Kim, D. Seol, S. Lee, H. N. Lee, and Y. Kim, Appl. Phys. Lett. **109**, 102901 (2016).
[14] R. Proksch, J. Appl. Phys. **116**, 066804 (2014).
[15] S. Jesse, A. Kumar, T. M. Arruda, Y. Kim, S. Kalinin, and F. Ciucci, MRS Bull. **37**, 651 (2012).
[16] C. Rivera, J. Appl. Phys. **109**, 013513 (2011).
[17] J. A. Tuszynski, T. J. A. Craddock, and E. J. Carpenter, J. Comput. Theor. Nanos. **5**, 2022 (2008).
[18] D. Jungbauer, Adv. Mater. **5**, 227 (1993).
[19] H. R. Leuchtag, *Voltage-Sensitive Ion Channels: Biophysics of Molecular Excitability*, Springer (Netherlands, 2008).
[20] T. Li, and K. Zeng, Acta Mater. **59**, 3667 (2011).
[21] M. Fang, K. G. Liroff, A. Simon Turner, C. M. Les, B. G. Orr, and M. M. B. Holl, J. Investig. Dermatol. **132**, 1791 (2012).
[22] X. Qiu, L. Holländer, W. Wirges, R. Gerhard, and H. C. Basso, J. Appl. Phys. **113**, 224106 (2013).
[23] P. Hu, S. Hu, Y. Huang, J. R. Reimers, A. M. Rappe, Y. Li, A. Stroppa, and W. Ren, J. Phys. Chem. Lett. **10**, 1319 (2019).
[24] H. R. Leuchtag, and V. S. Bystrov, Ferroelectrics **220**, 157 (1999).
[25] H. R. Leuchtag, and V. S. Bystrov, Ferroelectrics **220**, 5 (1999).
[26] J. Tuszynski, T. Craddock, and E. J. Carpenter, J. Comput. Theor. Nanos. **5**, 2022 (2008).
[27] A. L. Galvani, Clin. Orthop. Relat. Res. **88**, 2 (1972).
[28] A. J. P. Martin, Proc. Phys. Soc. **53**, 186 (1941).
[29] V. A. Bazhenov, *Piezoelectric Properties of Wood*, Consultants Bureau (New York, 1961).
[30] E. Fukada, Nature **166**, 772 (1950).
[31] E. Fukada, J. Phys. Soc. Jpn. **10**, 149 (1955).
[32] E. Fukada, and I. Yasuda, J. Phys. Soc. Jpn. **12**, 1158 (1957).
[33] F. Eiichi, and Y. Iwao, Jpn. J. Appl. Phys. **3**, 117 (1964).
[34] W. S. Williams, and L. Breger, J. Biomech. **8**, 407 (1975).
[35] S. B. Lang, A. A. Marino, G. Berkovic, M. Fowler, and K. D. Abreo, Bioelectrochem. Bioenerg. **41**, 191 (1996).
[36] A. Gruverman, B. Rodriguez, and S. Kalinin, JSPM **1**, 74 (2006).
[37] A. A. Marino, and B. D. Gross, Arch. Oral Biol. **34**, 507 (1989).
[38] S. B. Lang, Nature **212**, 704 (1966).
[39] V. V. Lemanov, in *Piezoelectric Materials: Advances in Science, Technology and Applications*, edited by C. Galassi, M. Dinescu, K. Uchino, and M. Sayer (Kluwer Academic Publishers, Dordrecht, The Netherlands, 2000), pp. 1-9.
[40] H. Fröhlich, La Rivista del Nuovo Cimento (1971-1977) **7**, 399 (1977).
[41] T. Li, and K. Zeng, J. Appl. Phys. **113**, 187202 (2013).
[42] J. Jacob, N. More, K. Kalia, and G. Kapusetti, Inflamm. Regener. **38**, 2 (2018).
[43] N. Amdursky, P. Beker, J. Schklovsky, E. Gazit, and G. Rosenman, Ferroelectrics **399**, 107 (2010).
[44] H. Athenstaedt, Ferroelectrics **11**, 365 (1976).
[45] E. Fukada, Q. Rev. Biophys. **16**, 59 (2009).
[46] E. Kalmykova, and C. A. Mgina, Tanz. J. Sci. **38**,

209 (2012).
[47] H. Athenstaedt, Ann. N. Y. Acad. Sci. **238**, 68 (1974).
[48] P. Jiang, F. Yan, E. N. Esfahani, S. Xie, D. Zou, X. Liu, H. Zheng, and J. Li, ACS Biomater. Sci. Eng. **3**, 1827 (2017).
[49] S. B. Lang, Nature **224**, 798 (1969).
[50] G. W. Hastings, M. A. ElMessiery, and S. Rakowski, Biomaterials **2**, 225 (1981).
[51] A. A. Marino, and R. O. Becker, Nature **228**, 473 (1970).
[52] A. A. Marino, R. O. Becker, and S. C. Soderholm, Calcif. Tissue Res. **8**, 177 (1971).
[53] N. C. Abascal, and L. Regan, Open Biol. **8**, 180113 (2018).
[54] H. Athenstaedt, Nature **228**, 830 (1970).
[55] A. Hosokawa, J. Acoust. Soc. Am. **140**, EL441 (2016).
[56] G. Hastings, M. ElMessiery, and S. Rakowski, Biomaterials **2**, 225 (1981).
[57] M. H. Shamos, L. S. Lavine, and M. I. Shamos, Nature **197**, 81 (1963).
[58] E. Fukada, H. Ueda, and R. Rinaldi, Biophys. J. **16**, 911 (1976).
[59] E. Korostoff, J. Biomech. **10**, 41 (1977).
[60] A. Ferreira, G. González, R. González-Paz, J. Feijoo, J. Lira-Olivares, and K. Noris-Suárez, Acta Microsc. **18**, 278 (2009).
[61] J. C. Góes, S. D. Figueiró, J. A. C. De Paiva, I. F. De Vasconcelos, and A. S. B. Sombra, J. Mater. Sci. Lett. **18**, 983 (1999).
[62] E. Fukada, IEEE Trans. Ultrason. Ferroelectr. Freq. Control **47**, 1277 (2000).
[63] E. Fukada, and K. Hara, J. Phys. Soc. Jpn. **26**, 777 (1969).
[64] Y. Liu, H.-L. Cai, M. Zelisko, Y. Wang, J. Sun, F. Yan, F. Ma, P. Wang, Q.N. Chen, H. Zheng, X. Meng, P. Sharma, Y. Zhang, and J. Li, Proc. Natl. Acad. Sci. U. S. A. **111**, E2780 (2014).
[65] Y. Zhao, H. Fan, X. Ren, C. Long, G. Liu, and Z. Liu, J. Mater. Chem. C **4**, 7324 (2016).
[66] C. M. Kelly, T. Northey, K. Ryan, B. R. Brooks, A. L. Kholkin, B. J. Rodriguez, and N. -V. Buchete, Biophys. Chem. **196**, 16 (2015).
[67] R. A. Kumar, R. E. Vizhi, N. Vijayan, and D. R. Babu, Physica B Condens. Matter **406**, 2594 (2011).
[68] T. Yucel, P. Cebe, and D. L. Kaplan, Adv. Funct. Mater. **21**, 779 (2011).
[69] V. V. Lemanov, S. N. Popov, and G. A. Pankova, Phys. Solid State **44**, 1929 (2002).
[70] V. V. Lemanov, S. G. Shul'man, V. K. Yarmarkin, S. N. Popov, and G. A. Pankova, Phys. Solid State **46**, 1285 (2004).
[71] S. Kim, and S. -J. Choi, Anal. Biochem. **458**, 1 (2014).
[72] V. S. Bystrov, E. Seyedhosseini, I. K. Bdikin, S. Kopyl, A. L. Kholkin, S. G. Vasilev, P. S. Zelenovskiy, D. S. Vasileva, and V. Y. Shur, Ferroelectrics **496**, 28 (2016).
[73] D. Vasilescu, R. Cornillon, and G. Mallet, Nature **225**, 635 (1970).
[74] R. L. Bunde, E. J. Jarvi, and J. J. Rosentreter, Talanta **51**, 159 (2000).
[75] A. S. Nuraeva, D. S. Vasileva, S. G. Vasilev, P. S. Zelenovskiy, D. A. Gruzdev, V. P. Krasnov, V. A. Olshevskaya, V. N. Kalinin, and V. Y. Shur, Ferroelectrics **496**, 1 (2016).
[76] B. J. Rodriguez, A. Gruverman, A. Kingon, R. Nemanich, and O. Ambacher, Appl. Phys. Lett. **80**, 4166 (2002).
[77] A. N. Morozovska, S. V. Svechnikov, E. A. Eliseev, S. Jesse, B. J. Rodriguez, and S. V. Kalinin, J. Appl. Phys. **102**, 114108 (2007).
[78] B. J. Rodriguez, S. Jesse, S. V. Kalinin, J. Kim, S. Ducharme, and V. Fridkin, Appl. Phys. Lett. **90**, 122904 (2007).
[79] Y. Liu, D. N. Weiss, and J. Li, ACS Nano **4**, 83 (2010).
[80] A. Gruverman, D. Wu, B. J. Rodriguez, S. V. Kalinin, and S. Habelitz, Biochem. Biophys. Res. Commun. **352**, 142 (2007).
[81] S. Habelitz, B. Rodriguez, S. Marshall, G. Marshall, S. V. Kalinin, and A. Gruverman, J. Dent. Res. **86**, 908 (2007).
[82] C. Halperin, S. Mutchnik, A. Agronin, M. Molotskii, P. Urenski, M. Salai, and G. Rosenman, Nano Lett. **4**, 1253 (2004).
[83] S. V. Kalinin, B. J. Rodriguez, S. Jesse, T. Thundat, and A. Gruverman, Appl. Phys. Lett. **87**, 053901 (2005).
[84] M. Minary-Jolandan, and M. -F. Yu, Appl. Phys. Lett. **97**, 153127 (2010).
[85] V. R. Binetti, J. D. Schiffman, O. D. Leaffer, J. E. Spanier, and C. L. Schauer, Integr. Biol. **1**, 324 (2009).
[86] D. Denning, J. I. Kilpatrick, E. Fukada, N. Zhang, S. Habelitz, A. Fertala, M. D. Gilchrist, Y. Zhang, S. A. M. Tofail, and B. J. Rodriguez, ACS Biomater. Sci. Eng. **3**, 929 (2017).
[87] I. Bdikin, V. Bystrov, S. Kopyl, R. P. Lopes, I. Delgadillo, J. Gracio, E. Mishina, A. Sigov, and A. L. Kholkin, Appl. Phys. Lett. **100**, 043702 (2012).
[88] A. Heredia, V. Meunier, I. K. Bdikin, J. Gracio, N. Balke, S. Jesse, A. Tselev, P. K. Agarwal, B. G. Sumpter, and S. V. Kalinin, Adv. Funct. Mater. **22**, 2996 (2012).
[89] A. Kholkin, N. Amdursky, I. Bdikin, E. Gazit, and G. Rosenman, ACS Nano **4**, 610 (2010).
[90] Y. Liu, Y. Zhang, M. -J. Chow, Q. N. Chen, and J. Li, Phys. Rev. Lett. **108**, 078103 (2012).
[91] E. Beniash, Wiley Interdiscip. Rev. Nanomed. Nanobiotechnol. **3**, 47 (2011).
[92] T. Li, and K. Zeng, Adv. Mater. **30**, 1803064 (2018).
[93] T. Li, L. Chen, and K. Zeng, Acta Biomater. **9**, 5903

(2013).
[94] H. Zhou, J. Hong, Y. Zhang, F. Li, Y. Pei, and D. Fang, Physica B Condens. Matter **407**, 3377 (2012).
[95] C. Harnagea, M. Vallières, C.P. Pfeffer, D. Wu, B.R. Olsen, A. Pignolet, F. Légaré, and A. Gruverman, Biophys. J. **98**, 3070 (2010).
[96] M. -J. Majid, and Y. Min-Feng, Nanotechnology **20**, 085706 (2009).
[97] M. Minary-Jolandan, and M. -F. Yu, ACS Nano **3**, 1859 (2009).
[98] M. Lallart, J. -F. Capsal, G. Sebald, P. -J. Cottinet, and D. Guyomar, Sensor. Actuat. B-Chem. **190**, 259 (2014).
[99] S. Kim, D. Seol, X. Lu, M. Alexe, and Y. Kim, Sci. Rep. **7**, 41657 (2017).
[100] N. Balke, S. Jesse, P. Yu, C. Ben, S. V. Kalinin, and A. Tselev, Nanotechnology **27**, 425707 (2016).
[101] R. S. Dahiya, and M. Valle, *Robotic Tactile Sensing-Technologies and System*, Springer (Netherlands, 2013).
[102] S. Guerin, S. A. M. Tofail, and D. Thompson, NPG Asia Mater. **11**, 10 (2019).
[103] P. A. Williams, C. E. Hughes, and K. D. M. Harris, Angew. Chem. Int. Ed. **54**, 3973 (2015).
[104] A. Stapleton, M. R. Noor, J. Sweeney, V. Casey, A. L. Kholkin, C. Silien, A. A. Gandhi, T. Soulimane, and S. A. M. Tofail, Appl. Phys. Lett. **111**, 142902 (2017).
[105] S. Guerin, A. Stapleton, D. Chovan, R. Mouras, M. Gleeson, C. McKeown, M. R. Noor, C. Silien, F. M. F. Rhen, Andrei L. Kholkin, N. Liu, T. Soulimane, S. A. M. Tofail, and D. Thompson, Nat. Mater. **17**, 180 (2017).
[106] S. Guerin, T. A. M. Syed, and D. Thompson, Nanoscale **10**, 9653 (2018).
[107] D. N. LeBard, and D. V. Matyushov, J. Phys. Chem. B **114**, 9246 (2010).
[108] W. Känzig, *Solid State Physics: Advances in Research and Applications*, Academic Press Inc. (U.S., 1957).
[109] A. M. Glass, and M. E. Lines, *Principles and Applications of Ferroelectrics and Related Materials*, Clarendon Press (Oxford, 1977).
[110] J. Li, Y. Liu, Y. Zhang, H.-L. Cai, and R.-G. Xiong, Phys. Chem. Chem. Phys. **15**, 20786 (2015).
[111] Y. Liu, Y. Wang, M. -J. Chow, N. Q. Chen, F. Ma, Y. Zhang, and J. Li, Phys. Rev. Lett. **110**, 168101 (2013).
[112] H. Athenstaedt, Nat. Sci. **48**, 465 (1961).
[113] Y. Sun, Y. Cheng, and K. Y. Zeng, in *Layered Materials for Energy Storage and Conversion*, edited by D. Geng, Y. Cheng, and G. Zhang (The Royal Society of Chemistry, United Kingdom, 2019), pp. 197-244.
[114] J. K. Sinha, J. Sci. Instrum. **42**, 696 (1965).
[115] A. Gruverman, M. Alexe, and D. Meier, Nat. Commun. **10**, 1661 (2019).
[116] A. L. Kholkin, S. V. Kalinin, A. Roelofs, and A. Gruverman, in *Scanning Probe Microscopy: Electrical and Electromechanical Phenomena at the Nanoscale*, edited by S. Kalinin, and A. Gruverman (Springer, New York, 2007), pp. 173-214.
[117] S. V. Kalinin, A. N. Morozovska, L. Q. Chen, and B. J. Rodriguez, Rep. Prog. Phys. **73**, 056502 (2010).
[118] S. Jesse, H. N. Lee, and S. V. Kalinin, Rev. Sci. Instrum. **77**, 073702 (2006).
[119] S. Jesse, A. P. Baddorf, and S. V. Kalinin, Appl. Phys. Lett. **88**, 062908 (2006).
[120] F. Libonati, and L. Vergani, Compos. Struct. **139,** 188 (2016).
[121] B. Schwenzer, and K. -H. van Pée, Angew. Chem. Int. Ed. **43**, 1045 (2004).
[122] C. Gistelinck, R. Gioia, A. Gagliardi, F. Tonelli, L. Marchese, L. Bianchi, C. Landi, L. Bini, A. Huysseune, P. E. Witten, A. Staes, K. Gevaert, N. De Rocker, B. Menten, F. Malfait, S. Leikin, S. Carra, R. Tenni, A. Rossi, A. De Paepe, P. Coucke, A. Willaert, and A. Forlino, Sci. Rep. **6**, 21540 (2016).
[123] J. Uitto, Arch. Biochem. Biophys. **192**, 371 (1979).
[124] S. -W. Chang, S. J. Shefelbine, and M. J. Buehler, Biophys. J. **102**, 640 (2012).
[125] D. Denning, J. Guyonnet, and B. J. Rodriguez, Int. Mater. Rev. **61**, 46 (2016).
[126] M. Fang, and M. M. Holl, BoneKey Rep. **21**, 394 (2013).
[127] J. P. R. O. Orgel, T. C. Irving, A. Miller, and T. J. Wess, Proc. Natl. Acad. Sci. **103**, 9001 (2006).
[128] B. Vrhovski, and A. S. Weiss, Eur. J. Biochem. **258**, 1 (1998).
[129] C. A. Gibbons, and R. E. Shadwick, J. Exp. Biol. **158**, 275 (1991).
[130] R. E. Shadwick, J. Exp. Biol. **202**, 3305 (1999).
[131] D. W. Urry, T. Hugel, M. Seitz, H. E. Gaub, L. Sheiba, J. Dea, J. Xu, T. Parker, A. J. Bailey, J. Macmillan, P. R. Shrewry, and A. S. Tatham, Philos. Trans. R. Soc. Lond. B Biol. Sci. **357**, 169 (2002).
[132] C. A. J. Hoeve, and P. J. Flory, Biopolymers **13**, 677 (1974).
[133] B. B. Aaron, and J. M. Gosline, Biopolymers **20**, 1247 (1981).
[134] S. Rauscher, S. Baud, M. Miao, F. W. Keeley, and R. Pomès, Structure **14**, 1667 (2006).
[135] S. Rauscher, C. Neale, and R. Pomès, J. Chem.Theory Comput. **5**, 2640 (2009).
[136] S. Rauscher, and R. Pomès, in *Fuzziness: Structural Disorder in Protein Complexes*, edited by M. Fuxreiter, and P. Tompa (Springer, New York, 2012), pp. 159-183.
[137] A. A. Marino, J. A. Spadaro, E. Fukada, L. D. Kahn, and R. O. Becker, Calcif. Tissue Int. **31**, 257 (1980).

[138] D. Denning, M. V. Paukshto, S. Habelitz, and B. J. Rodriguez, J. Biomed. Mater. Res. B Appl. Biomater. **102**, 284 (2014).
[139] V. O. Neto, C. Silva, A. F. L. Almeida, S. D. Figueiró, J. Góes, C. Magalhaes, and S. Sombra, Solid State Sci. **4**, 43 (2002).
[140] A. Todorov, A. Petrov, and J. Fendler, Langmuir **10**, 2344 (1994).
[141] S. M. Mithieux, and A. S. Weiss, Adv. Protein Chem. **70**, 437 (2005).
[142] J. H. Kristensen, and M. A. Karsdal, in *Biochemistry of Collagens, Laminins and Elastin*, edited by M. A. Karsdal (Academic Press, U. S. 2016), pp. 197-201.
[143] C. -A. Couture, S. Bancelin, J. Van der Kolk, K. Popov, M. Rivard, K. Légaré, G. Martel, H. Richard, C. Brown, S. Laverty, L. Ramunno, and F. Légaré, Biophys. J. **109**, 2501 (2015).
[144] J. Bella, M. Eaton, B. Brodsky, and H. Berman, Science **266**, 75 (1994).
[145] M. S. Pometun, E. Y. Chekmenev, and R. J. Wittebort, J. Biol. Chem. **279**, 7982 (2004).
[146] F. Li, L. Jin, Z. Xu, and S. Zhang, Appl. Phys. Rev. **1**, 011103 (2014).
[147] U. K. Bhaskar, N. Banerjee, A. Abdollahi, Z. Wang, D. G. Schlom, G. Rijnders, and G. Catalan, Nat. Nanotechnol. **11**, 263 (2015).
[148] W. Ma, Phys. Status Solidi B **245**, 761 (2008).
[149] P. Kumar, Y. G. Marinov, H. P. Hinov, U. S. Hiremath, C. V. Yelamaggad, K. S. Krishnamurthy, and A. G. Petrov, J. Phys. Chem. B **113**, 9168 (2009).
[150] K. D. Breneman, W. E. Brownell, and R. D. Rabbitt, PLOS One **4**, e5201 (2009).
[151] A. G. Petrov, *Physical and Chemical Bases of Biological Information Transfer*, Plenum Press (New York, 1975).
[152] J. Hong, and D. Vanderbilt, Phys. Rev. B **84**, 180101 (2011).
[153] R. Resta, Phys. Rev. Lett. **105**, 127601 (2010).
[154] R. Maranganti, N. D. Sharma, and P. Sharma, Phys. Rev. B **74**, 014110 (2006).
[155] G. Schulze, F. Jona and G. Shirane, J. Appl. Math. Mech. **43**, 512 (1963).
[156] A. K. Tagantsev, Phys. Rev. B **34**, 5883 (1986).
[157] A. K. Tagantsev, Phase Transit. **35**, 119 (1991).
[158] A. Abdollahi, F. Vásquez-Sancho, and G. Catalan, Phys. Rev. Lett. **121**, 205502 (2018).
[159] Z. Yan, and L. Jiang, J. Phys. D Appl. Phys. **46**, 355502 (2013).
[160] L. Chu, Y. Li, and G. Dui, Acta Mech. **230**, 3071 (2019).
[161] A. Gomez, T. Puig, and X. Obradors, Appl. Surf. Sci. **439**, 577 (2018).
[162] N. Balke, S. Jesse, B. Carmichael, M. B. Okatan, I. I. Kravchenko, S. V. Kalinin, and A. Tselev, Nanotechnology **28**, 065704 (2017).
[163] B. J. Rodriguez, C. Callahan, S. V. Kalinin, and R. Proksch, Nanotechnology **18**, 475504 (2007).
[164] N. C. Miller, H. M. Grimm, W. S. Horne, and G. R. Hutchison, Nanoscale Adv. **1**, (4834) (2019).
[165] C. W. Marvin, H. M. Grimm, N. C. Miller, W. S. Horne, and G. R. Hutchison, J. Phys. Chem. B **121**, 10269 (2017).
[166] E. A. Eliseev, A. N. Morozovska, A. V. Ievlev, N. Balke, P. Maksymovych, A. Tselev, and S. V. Kalinin, Appl. Phys. Lett. **104**, 232901 (2014).
[167] D. Seol, S. Park, O. V. Varenyk, S. Lee, H. N. Lee, A. N. Morozovska, and Y. Kim, Sci. Rep. **6**, 30579 (2016).
[168] Q. N. Chen, Y. Ou, F. Ma, and J. Li, Appl. Phys. Lett. **104**, 242907 (2014).
[169] K. Chu, B. -K. Jang, J. H. Sung, Y. A. Shin, E. -S. Lee, K. Song, J. H. Lee, C. -S. Woo, S. J. Kim, S. -Y. Choi, T. Y. Koo, Y. -H. Kim, S. -H. Oh, M. -H. Jo, and C. -H. Yang, Nat. Nanotechnol. **10**, 972 (2015).
[170] S. Hu, H. Li, and H. Tzou, J. Intell. Material Syst. Struct. **25**, 832 (2014).
[171] S. V. Kalinin, S. Jesse, W. Liu, and A. A. Balandin, Appl. Phys. Lett. **88**, 153902 (2006).
[172] P. -C. Zhang, A. M. Keleshian, and F. Sachs, Nature **413**, 428 (2001).
[173] A. G. Moura, and A. Erturk, J. Intell. Material Syst. Struct. **29**, 3949 (2018).
[174] D. Yao, H. Zhou, X. Wang, and J. Hong, in *2017 Symposium on Piezoelectricity, Acoustic Waves, and Device Applications (SPAWDA)*, 27-30 October 2017, Chengdu, China, pp. 325-330.
[175] X. Zhuang, B. He, B. Javvaji, and H. S. Park, Phys. Rev. B **99**, 054105 (2019).
[176] B. H. Nguyen, S. S. Nanthakumar, X. Zhuang, P. Wriggers, X. Jiang, and T. Rabczuk, Eur. J. Mech. A Solids **71**, 404 (2018).
[177] A. S. Tayi, A. K. Shveyd, A. C. H. Sue, J. M. Szarko, B. S. Rolczynski, D. Cao, T. J. Kennedy, A. A. Sarjeant, C. L. Stern, W. F. Paxton, W. Wu, S. K. Dey, A. C. Fahrenbach, J. R. Guest, H. Mohseni, L. X. Chen, K. L. Wang, J. F. Stoddart, and S. I. Stupp, Nature **488**, 485 (2012).